Food Chemistry 512 (2026) 148910

Contents lists available at ScienceDirect

Food Chemistry

journal homepage: www.elsevier.com/locate/foodchem

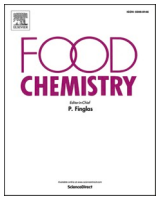

The interaction between egg white and faba bean protein during the heat-induced gelling process and its effects on textural, rheological, and structural properties

Fangzhou Wang [a,*], Romdhane Karoui [b], Christophe Blecker [a]

[a] Gembloux Agro-Bio Tech, Department of Food Science and Formulation, University of Liège, 5030 Gembloux, Belgium
[b] Univ. Artois, Univ. Lille, Univ. Littoral Côte d'Opale, Univ. Picardie Jules Verne, Univ. de Liège, INRAE, Junia, UMR-T 1158, BioEcoAgro, F-62300 Lens, France

ARTICLE INFO

Keywords:
Gelling properties
Egg white
Faba bean protein
Protein-protein interaction
Microstructure

ABSTRACT

The interaction between egg white (EW) and faba bean protein (FP) observed during the heat-inducing gelling process impaired the properties of the final products, which cannot be neglected in food processing. In this study, protein behaviors during gelation and the structural characterization of gel matrix in EW/FP ratios of 10:0, 8:2, 6:4, 4:6, 2:8, and 0:10 were investigated to explore the mechanism. The results showed that the EW-FP interaction increased the protein surface hydrophobicity during gelation than the predicted linear change by 7.28%, 11.45%, 13.11%, and 5.43% in groups 8:2, 6:4, 4:6, and 2:8, respectively, which led to asynchronous network formation and further delivered a microstructure with more porosity and a higher proportion of free water. Meanwhile, higher ratios of hydrophobic interaction and fewer disulfide bonds were detected in the composite gel's structure. This series of chain reactions caused patterned losses in texture and water-holding capacity.

1. Introduction

The partial substitution of animal-based protein using plant-based protein nowadays is widely used in food industries to lower the cost of production and to meet the increasing consumption, as well as to achieve the goal of sustainable development (Augustin & Cole, 2022). Animal-based proteins such as milk, eggs, meat, and seafood remain the most important protein sources, which offer numerous advantages from nutritional, sensory, and functional perspectives that cannot be completely replaced by plant-based protein (Alves & Tavares, 2019; Day, 2013; Silva et al., 2019). The partial replacement by plant-based protein not only reduces the usage amount of animal protein but also has great potential to introduce novel functional properties into the complex system (Wu et al., 2019; Wu et al., 2021). Moreover, novel properties arise from the interaction between different protein fractions, which occurs when there are two or more types in a mixing system. An increasing number of studies have focused on this, which promoted partial substitution into realistic production (Alves & Tavares, 2019; Grasberger et al., 2021; Lin et al., 2017; Su et al., 2015; Ye et al., 2024; Zou et al., 2025), including the research of composite protein gels, which were from the perspective to take advantage of the excellent gelling function from both animal and plant-based proteins.

Faba bean (broad bean, *Vicia faba* L.), as a future source of protein, is regarded as a sustainable agricultural product because of its better symbiotic nitrogen fixation ability than other legumes and the high protein content (32–36%), which is almost twice that of cereal grains (Manickavasagan & Thirunathan, 2020; Rahate et al., 2021). Also, it is one of the cheapest sources of lysine-rich protein (Punia Bangar & Bala Dhull, 2022). Furthermore, Faba protein (FP) presented excellent gelling properties according to previous studies. Johansson et al. (2023) demonstrated the different gelling properties between 7S and 11S globulin fractions from faba and the changes in rheology, mechanical properties, and microstructure with the different NaCl additions. Langton et al. (2020) concluded that the finest gel microstructure can be obtained at pH 7 independent of the extraction method and NaCl concentration. While Guldiken et al. (2021) found that both NaCl and $CaCl_2$ could strengthen the network. In addition, FP could form a gel with significantly lower protein concentration compared to soy and pea, and the highest values on water and oil absorption (Fernández-Quintela et al., 1997). As well, Kim and Chin (2024) reported that FP showed good water-holding capacity (WHC) as an addition to meat products. Therefore, for the preparation of food gel products, introducing FP into animal protein can be used as a way to develop its application.

Egg white (EW) is a widely used protein in people's daily lives, and its

* Corresponding author.
E-mail address: fangzhou.wang@doct.uliege.be (F. Wang).

https://doi.org/10.1016/j.foodchem.2026.148910
Received 15 January 2025; Received in revised form 3 February 2026; Accepted 15 March 2026
Available online 17 March 2026

commercial products are also an important raw material in the food industry. The heat-induced gelling process was well understood by a great number of studies. Under the heating process, the protein molecules firstly partially unfold to aggregate via intermolecular β-sheet with the consumption of helical structure, and further cross-link to gel network driven by the surface hydrophobicity and disulfide bonds (Li et al., 2018). The protein fractions of ovalbumin and ovotransferrin have dominant effects on the formation of the network (Croguennec et al., 2007). Furthermore, a few studies have attempted to mix it with legume proteins to investigate the gelling properties. Su et al. (2015) blended the egg white with soy protein to prepare the composite gel, where the texture, WHC, and microstructure were investigated, and the 1:1 ratio group had the highest springiness and WHC. Zhao et al. (2024) considered the mixing of EW and pea protein isolate and obtained a gel with a denser microstructure in which the EW acted as a filler in the pea protein network. The WHC was also improved with the 5:1 ratio of pea protein-EW. However, a phase separation of the gel structure was also presented in the EW-pea protein composite gel, where pea protein promoted the formation of aggregates embedded in the EW network and loosened the gel strength (Kuang et al., 2025). Both synergistic and antagonistic effects were observed in the composite gels when mixing EW and legume protein, such as soy and pea. Nevertheless, the gelling properties of mixing EW with FP have not been explored yet, and the partial substitution is worth comprehensively investigating before utilization to exert its potential for food products, such as protein bars, puddings, and the filling of sandwich biscuits, as well as the medical uses such as drug delivery and dysphagia food (Li et al., 2025; Ozcan et al., 2023; Thakur et al., 2018).

The aim of the present study was to investigate the gelling properties of the EW-FP composite gels as influenced by the mixing ratio, and to determine whether synergistic or antagonistic effects occur in their textural properties and WHC. In addition, changes in protein structure and intermolecular interactions were examined to elucidate the mechanisms of gel formation and the nature of the interactions between EW and FP.

To address these objectives, composite gels were prepared using different EW: FP protein ratios (respectively 10:0, 8:2, 6:4, 4:6, 2:8, and 0:10). The textural profile analysis, rheology, and WHC were performed on the mixed protein gels. The fluorescence spectroscopy, mid-infrared spectroscopy, scanning electron microscopy (SEM), low-field nuclear magnetic resonance (LF-NMR), and determination of the intermolecular forces were exploited to understand the changes in protein structure and the EW-FP interactions.

2. Materials and methods

2.1. Materials

The liquid pasteurized egg white (10.71 g protein, 0.20 g fat, 0.81 g carbohydrate per 100 g) was supplied by Lodewijckx Group & Cocovite (Laakdal, Belgium) and freeze-dried before use. Faba bean (*Vicia faba* L. *v*ar. Nebraska) was cultivated in Germany and sampled during the 2017 agriculture campaign.1-Anilinonaphthalene-8-sulfonic acid (ANS) was purchased from Cayman Chemical Company (supplier – Sanbio B·V, Netherlands). All other chemicals were analytical grade.

2.2. Wet extraction and composition characterization of FP

The wet fractionation of the faba protein concentrates was referred to the method of Dumoulin et al. (2021) and Nahimana et al. (2023) with some modifications. Briefly, 184.50 g faba bean was first dehulled in a TM05 test Mill (Satake Corporation, Hiroshima, Japan), 15 s per run, then milled below 1 mm (PULVERISETTE 19, Fritsch, Germany), 32.07 g hulls and 136.50 g flour were obtained. The faba bean flour was dispersed in distilled water with the flour: water ratio of 1:10 *w/v* and vigorously stirred for 30 min. Then, the pH has been adjusted to 9.5 with 2 M NaOH and stirred for 30 min for the alkaline extraction. Liquid and solid were separated by centrifugation (14,300 $\times g$, 30 min, 4 °C). The acid precipitation of the supernatant was performed by adjusting to pH 4.5 with 2 M HCl and stirring for 30 min, and the precipitated protein was separated by centrifugation (14,300 $\times g$, 30 min, 4 °C). The collected protein fraction was then dissolved in 500 mL Milli-Q water, and the pH was adjusted to 7.0. The obtained neutral proteins were freeze-dried and ground into powder, 24.94 g protein concentrates were obtained. The extraction process was repeated 3 times to have enough FP for the following experiments.

The protein content of FP was determined by the Dumas method (N $\times$ 6.25) using Elementar (Rapid N Exceed). The fat and fiber content was performed according to Commission Regulation (EC) No.152/2009, in terms of "H. Determination of Crude Oils and Fats", and "I. Determination of crude fiber". The total starch was determined using a Total Starch HK assay kit (Megazyme, Wicklow, Ireland). The compositions by weight of FP are listed as follows: dry matter 97.12 $\pm$ 0.06%, protein 82.16 $\pm$ 0.67%, fat 5.03 $\pm$ 0.12%, fiber 0.16 $\pm$ 0.01%, starch 1.05 $\pm$ 0.00%, ash 6.56 $\pm$ 0.01%.

2.3. Preparation of gels

The gels (12% *w*/w protein) were prepared according to the methods of Li et al. (2023) and Guldiken et al. (2021) with some modifications. BrieflyBriefly, the EW and FP powders were mixed in the ratios of 10:0, 8:2, 6:4, 4:6, 2:8, and 0:10, respectively (based on the protein mass) and were well dispersed in Milli-Q water. Next, the dispersions were adjusted to pH 7.0 with tiny amounts of 2 M NaOH and hydrated overnight at 4 °C under stirring. Then, the dispersions were carefully poured into 50 mL beakers (38 mm $\times$ 66 mm) while avoiding the foam being poured with the solution. The gelling process was performed by heating the beakers in a 95 °C water bath for 20 min and cooling them in an ice-water bath for 15 min, and after, gels were placed in 4 °C for 24 h before analysis.

2.4. Textural profile analysis

The gels prepared in section 2.3 were taken out from beakers by a hollow thin-walled metal tube (inner diameter 20 mm) and trimmed with fishing wire into a diameter 20 mm $\times$ height 13 mm cylinders. The textural profile was determined by TA XT2 Texture Analyzer (Stable Micro Systems, Godalming, UK) fitted with a 35-mm-diameter metal plunger (P/35, 35 mm diameter cylinder aluminum) according to the method of Li et al. (2018) and Blecker et al. (2000) with some modifications. Gel samples were subjected to 50% deformation with the crosshead speed of 1 mm/s, 5 s interval between two compression cycles. Hardness was defined as the peak force of the first compression. Resilience is calculated by dividing the upstroke force area of the first compression by the downstroke force area of the first compression. Cohesiveness was defined as the ratio of the positive area of the second compression to that of the first compression. Springiness was defined as the percentage of height that the samples recovered during the time elapsed between the end of the first bite and the start of the second bite. Gumminess was expressed as the product of hardness and cohesiveness.

2.5. WHC

The WHC (%) was determined according to the method of Blecker et al. (2000) with some modifications. The gel samples (around 8 g) were transferred to 50 mL centrifuge tubes (fitted with a plastic filter and an 11 μm filter paper to separate the pellet and water) and centrifuged at 10000 $\times g$ for 15 min at 4 °C. The WHC was expressed as the percentage of the pellet weight relative to the original weight of the gel.

2.6. Rheology

The rheological properties were measured based on the method of Li et al. (2023) with some modifications. The mixed EW-FP protein dispersions (total protein content 12% *w*/w) were characterized by the oscillatory test on the MCR 302 Rheometer (Anton Paar, Graz, Austria) fitted with a parallel plate and a PP50-SN30993 probe. The measuring gap was 1 mm, and silicon oil was used to prevent evaporation. For the temperature sweep (angular frequency of 1 Hz and strain of 0.1%), the samples were equilibrated at 25 °C for 1.5 min, then the temperature increased from 25 to 95 °C at the rate of 5 °C / min, maintained at 95 °C for 10 min, and then, cooled to 25 °C at the rate of 5 °C / min. The following dynamic frequency sweep was performed at 25 °C from 0.1 to 100 Hz at 0.1% strain. The storage modulus (G') and loss modulus (G") were recorded throughout the measurement. At the end of each measurement, an amplitude sweep was used to confirm the formed gel was performed within the linear viscoelastic region. The extrapolation method was used to identify the relative onset temperatures of the protein's gelation based on the G' curve during heating (Ma et al., 2023), where the temperature at the intersection of the tangent line along the baseline (initial G') and the tangent line at the steepest region of the G' was regarded as the onset temperature. Moreover, the power-law model ($G' = K^{*}\omega^{n'}$) was also curve-fitted with the frequency profile to elucidate the gelling properties where, ω is the frequency (Hz), K' indicates the sample's stiffness, and n' represents the relative amount of covalent bonds (the closer the value is to zero, the more covalent bonds the sample has).

2.7. Surface hydrophobicity and intrinsic fluorescence

One percent mixed EW-FP dispersions, which were much lower than the critical gelling concentration (4% *w*/w of EW and 11% w/w of FP), were heated according to the process in section 2.3 to simulate the intermediation state before the final formation of gels, where the surface hydrophobicity and intrinsic fluorescence were determined to describe the change of tertiary structure of protein molecules/aggregates and the microenvironment.

The surface hydrophobicity was determined according to the method of Diana Kerezsi et al. (2024) and Guldiken et al. (2021) with modifications. In brief, the mixed EW-FP dispersions were diluted into 0.005%, 0.010%, 0.015%, 0.020%, and 0.025% (*w*/w) using 10 mM sodium phosphate buffer (pH 7.0). For each concentration (0.005–0.025%), 1.6 mL of samples were mixed with 20 μL of 8 mM ANS solution (dissolved in 10 mM sodium phosphate buffer (pH 7.0)), then the samples were mixed well and reacted in the dark for 5 min. Fluorescence intensity (FI) was measured using a Fluoromax-4 spectrofluorometer (Jobin Yvon, Horiba, NJ, USA) equipped with a temperature controller (T Haake A25 AC200) with excitation and emission wavelengths of 390 and 470 nm, and the temperature of the measuring cell was kept at 25 °C, respectively. The slope of the maximum FI values against protein concentrations was calculated as the index of the protein surface hydrophobicity.

A null model was used to predict the surface hydrophobicity values of the mixed protein groups as $S_{predicted} = x \bullet S_{EW} + (1 - x) \bullet S_{FP}$, where x refers to the protein mass fraction of EW; S_{EW} and S_{FP} refer to the surface hydrophobicity of EW (group 10:0) and FP (group 0:10) (Zhao et al., 2024).

The intrinsic fluorescence of the dispersions was determined by the same spectrofluorometer as above, according to the method of Diana Kerezsi et al. (2024). 1% dispersions were incubated in a measuring cell for 3 min to reach the measuring temperature. Exciting wavelength was set at 290 nm, and the emission was collected between 305 and 450 nm.

2.8. Scanning electron microscopy (SEM)

The sample preparation before the SEM observation was conducted as the method of Wu et al. (2019). Gel samples were cut into thin slices (2 mm), and these cuboids were immersed in 2.5% glutaraldehyde for 48 h. Immobilized samples were rinsed with deionized water three times, then they were dehydrated by using a series of graded ethanol solutions ranging from 20% to 100% (*v*/v) and freeze-dried. The observation of the microstructure of protein gels was performed by the Scanning Electron Microscope FlexSEM 1000 II (Hitachi, Tokyo, Japan) at an acceleration voltage of 10 kV.

2.9. Middle field infrared

According to the method of Nahimana et al. (2023), the secondary structure of the mixed protein solution before gelling and the freeze-dried gel powder was analyzed using the Fourier Transform Infrared Spectroscopy method on the spectrometer IRTracer-100 (Shimazu, Duisburg, Germany). The samples were detected in a horizontal attenuated total reflectance (ATR) cell with zinc selenide crystal. The wavelength was in the range of 700–4000 cm^{-1}. The number of scans was 64 with a resolution of 16 cm^{-1}. The background of the solutions was Milli-Q water, and the background of the gel powders was air. The secondary structure was calculated by the LabSolution IR software (Easy Macro function).

2.10. Intermolecular forces in gels

The intermolecular forces were determined according to the method of Xia et al. (2022) with modifications. Briefly, different reagents were used to dissociate the gel structures by shielding different types of intermolecular forces as follows: reagent A (MiliQ water, as reference), reagent B (0.086 M Tris, 0.09 M glycine, 4 mM Na_2EDTA buffer, pH 8.0, to shield electrostatic interactions), reagent C (reagent B containing 1% SDS and 8 M urea, to disrupt hydrophobic interactions and hydrogen bonds), reagent D (reagent C containing 0.5% 2-mercaptoethanol, to break disulfide bonds). Gel samples were ground into fine pastes and placed in 50 mL centrifuge tubes with a sample size of 5.00 ± 0.01 g, and 10 mL dissociative reagents were added, respectively. Then the tubes were incubated for 48 h with string, then centrifuged at 15000 ×*g* for 10 min. The protein content of the supernatant was determined by the Pierce™ BCA protein Assay Kit - Reducing Agent compatible (Thermo Fisher Scientific Inc., Rockford, Illinois, USA). The gel solubility was calculated as the ratio of protein content in supernatant to the total protein content, and the solubility differences between different dissociative reagents reflected the proportions of different types of intermolecular force maintaining the gel structure (i.e., reagent B – reagent A, reagent C – reagent B, reagent D – reagent C).

2.11. Water distribution

T_2 relaxation time was determined by the MiniMR-60 LF-NMR analyzer (Niumag, Suzhou, China) equipped with a 0.5 T permanent magnet according to the method of Xie et al. (2024). The test conditions were set as follows: the proton resonance frequency, 23.2 MHz; the working temperature, 32 °C; the time waiting, 2000 ms; the time echo, 0.5 ms; the number of echoes, 12000; the number of scans, 4. Multi-exponential model within the MultiExp Inv Analysis program was used to analyze T2 distribution curves.

2.12. Statistical analysis

Significant differences ($p < 0.05$) in all data were determined by Duncan's multiple range test in one-way ANOVA on the software IBM SPSS Statistic (v29.0.1.0); Power-law fittings were analyzed using the least-squares method in scipy.optimize of Python package SciPy (v1.13.0) (Virtanen et al., 2020); Correlation analysis was determined by the Pearson method using the Python package Pandas (v2.2.2) (Team, T. Pandas Development, 2024); Figures were plotted with the Python package Matplotlib (v3.8.4) (Hunter, 2007). All measurements

were triplicated at least.

3. Results and discussion

3.1. Textural properties and WHC

3.1.1. Textural properties

The two-cycle compression was subjected to obtain the textual profiles of mixed EW-FP gels, and the results are shown in Fig. 1 (A, B, C, D, and E). EW gel (group 10:0, same as below) had high values of hardness, resilience, and gumminess, exhibiting a high strength, while those of FP gel (group 0:10, same as below) were significantly lower, exhibiting a low strength. Moreover, the values of springiness and cohesiveness of EW and FP gels were close. For the mixed groups, the hardness and gumminess decreased significantly with the increase in the ratio of FP, and the greatest decrease occurred between groups 8:2 and 6:4, and the decline rate slowed down at groups 4:6 and 2:8, presenting both concave trends between group 10:0 and 0:10. Besides, the gumminess, as the product of hardness and cohesiveness, is proportionally and significantly more impacted by hardness than cohesiveness. Also, the resilience and cohesiveness showed a slight "U" defection, and the groups 6:4 and 4:6 were the lowest, respectively. These concave and U-shaped trends exhibited the negative effects of mixing EW and FP on the textural properties. Except for the springiness, showing a synergic increase, group 4:6 had the highest value.

The results in this study are partially consistent with the study of Su et al. (2015), who substituted EW using soybean protein, presenting the highest springiness at a 1:1 ratio, which was in good agreement with the synergistically increased springiness of 6:4 and 4:6 groups in this study. However, Su et al. (2015) reported a linear change in hardness without synergistic behavior between EW and soybean protein, while the study of Zhao et al. (2024) reported that the composite gels of EW and pea protein exhibited synergistic increments in hardness for most of the mixing ratios. Differently, the EW-FP combination in this study exhibited the antagonistic effects in terms of all the textural parameters. It was concluded by many studies that textural properties are highly related to the homogeneity of microstructure (Johansson et al., 2024; Liu et al., 2024), and the asynchronous protein aggregation may be the reason that led to the heterogeneous gel and further defected the hardness, resilience, cohesiveness, and gumminess (Su et al., 2015), but the increase in springiness of the composited gels, maybe it was due to the porous structure generated provided the flexibility to gel.

3.1.2. WHC

WHC is one of the most important functional properties of heat-induced protein gels (Li et al., 2018). As shown in Fig. 1F, EW had a relatively low WHC, which was 63.75%, while FP showed a high value of 94.18%, indicating that the FP gel had an excellent WHC, which corresponded to the research of Johansson et al. (2024) where the FP gel had almost 100% WHC at pH 7.0 after the 5000 $\times g$ centrifugation. However, the mixed protein gel groups also exhibited a clear U-shaped trend of WHC; among them, group 8:2 had a reduced WHC of 58.47%, and group 6:4 had the lowest of 56.97%. For the following increase in FP content, the WHC showed an uptrend in groups 4:6 and 2:8, which were 63.16% and 76.1%, respectively. The results showed a negative interaction for WHC between EW and FP. Moreover, the WHC of protein gels is not only influenced by the coarseness of microstructure and the number of hydrogen bonds but also closely positively correlated to the textural properties (hardness) and the rheology (G') due to the stiffness of the gel structure, which prevents the water from being expelled under mechanical deformation (He et al., 2024; Min et al., 2022; Urbonaite et al., 2016; Xia et al., 2022). However, this study presented the opposite phenomenon: when the ratio of FP came to 40% and 80%, the WHC increased, while the hardness significantly decreased.

Based on the results, it was hypothesized that the change in texture and WHC originated from the protein-protein interaction during gel network formation. To explore the mechanism, the rheological temperature sweep, the determination of protein's intrinsic fluorescence and surface hydrophobicity were exploited to investigate the proteins' behavior during the gelling process; the determination of microstructure, secondary structure, intermolecular forces, water distribution, and rheological frequency sweep were used to characterize the structure of the gel matrix.

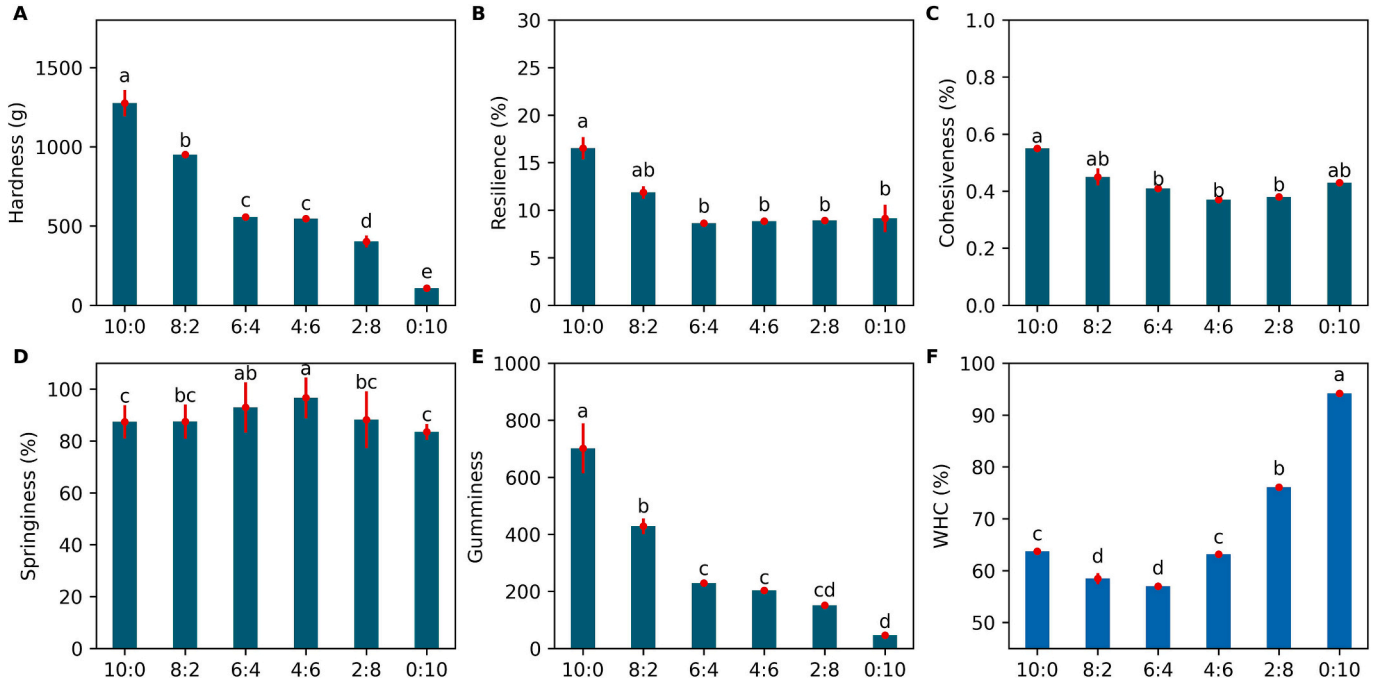

Fig. 1. The textural profile of hardness (A), resilience (B), cohesiveness (C), springiness (D), gumminess (E), and WHC (F) of the mixed EW-FP gels prepared in different ratios (The ratios in figures refer to the protein mass ratio of EW to FP). Different letters in each subplot represent significant differences ($p < 0.05$).

3.2. Protein behaviors during the gelling process

3.2.1. Oscillatory temperature sweep

The gelling process of the protein solution can be monitored by the temperature sweep, the denaturation and aggregation of protein fractions on the temperature ramp contributed to the formation of the gel structure, exhibiting the increase of the storage modulus (G') as shown in Fig. 2A. For the EW's gelling curve, there were two increasing G' regions: the "first slow-rising region" started around 66 °C, which was attributed to the denaturation and aggregation of ovotransferrin, and the "second rapid-rising region" was ovalbumin taking place around 78 °C (Li et al., 2023; Renzetti et al., 2020). Also, ovalbumin, which is the main gelling protein in the egg white, dominates the formation of the gel network (Razi et al., 2023). For the FP gelling process, the initiation temperature of G' was around 45 °C and steadily increased, then slowed at the 95 °C temperature platform, which highly corresponded to the study of Johansson et al. (2024). The denaturation temperature of 7S globulin (vicilin) and 11S globulin (legumin) can vary from 76.5 °C to 83.8 °C and 85.0 °C to 95.4 °C, respectively, depending on the ionic strength (Kimura et al., 2008). Nevertheless, those could not be identified in the G' curve in this study, also, each protein fraction's contribution to the G' increase is still not well understood by far. In addition, the G' of both EW and FP increased during the cooling stage, that of the EW group due to the formation of hydrogen bonds, which can combine more water into the protein structure and further strengthen the network (Wang et al., 2020). While the FP group, Johansson et al. (2022) reported the increase during cooling was also attributed to the presence of the starch (17.5–35% *w*/w), the amylose re-association and its network formation restrengthened the gel, whereas the starch content of the FP samples in this study was very low (1.05%). Hence, the mechanism of the increase in FP gel is likely the same as that given for EW gel.

For the mixed EW-FP groups, the overall storage modulus decreased with the increased FP ratio, and the thermal behaviors showed the combination of both EW and FP at different extents in terms of the initiation temperature around 45 °C featuring the FP group, the "slow-rising region" related to ovotransferrin, and the "rapid-rising region" related to ovalbumin. Besides, the main increase of G' of all mixed groups was more attributed to ovotransferrin and ovalbumin, which dominated the network formation by providing the backbone of the gel (Razi et al., 2023), while the FP acted more like a filler and diluted the network formed from EW to deliver a lower G' with the increase in its content. What is worth noting is, as shown in Table 1, the onset temperature of "slow-rising region" of all mixed groups became lower with the increase in FP content and dropped to 62 °C when the FP content reached 80%, as well, the "rapid-rising region" also exhibited advanced onset points of all mixed groups, which dropped from 79 °C to 70 °C when the FP content increased from 0 to 60%, and back to 73 °C in group 2:8. The earlier increase in G' related to ovotransferrin and ovalbumin indicated the interactions between FP and these two proteins, respectively, presenting that the denaturation and aggregation of these two proteins happened earlier. The advanced protein behavior also implied a faster and asynchronous aggregation during the gel formation. According to the correlation analysis (Supplementary Fig. 2), the onset temperature of ovotransferrin had highly significant correlations with the gel's mechanical properties in terms of hardness ($r = 0.972$, $p < 0.01$), resilience ($r = 0.961$, $p < 0.01$), cohesiveness ($r = 1.00$, $p < 0.01$), gumminess ($r = 0.985$, $p < 0.01$), final G' ($R^2 = 0.971$, $p < 0.01$), in the meantime, the onset temperature of ovalbumin also showed high correlation with hardness ($r = 0.894$, $p < 0.05$), resilience ($r = 0.896$, $p < 0.05$), cohesiveness($r = 0.925$, $p < 0.05$), gumminess ($r = 0.899$, $p < 0.05$), which can be concluded that the preinitiation of gelation can deliver changes to the gel structure and further affected the mechanical properties.

Moreover, Fig. 2B displays the increasing G" during the temperature sweep, by comparing with Fig. 2A, the rheological gelation point (G' > G") of most groups cannot be clearly identified because the EW protein had similar G' and G" at the beginning of the temperature sweep, and it showed the fluctuate curves under the unstable conditions when the temperature started to grow (The details of each group showed in Supplementary Fig. 1).

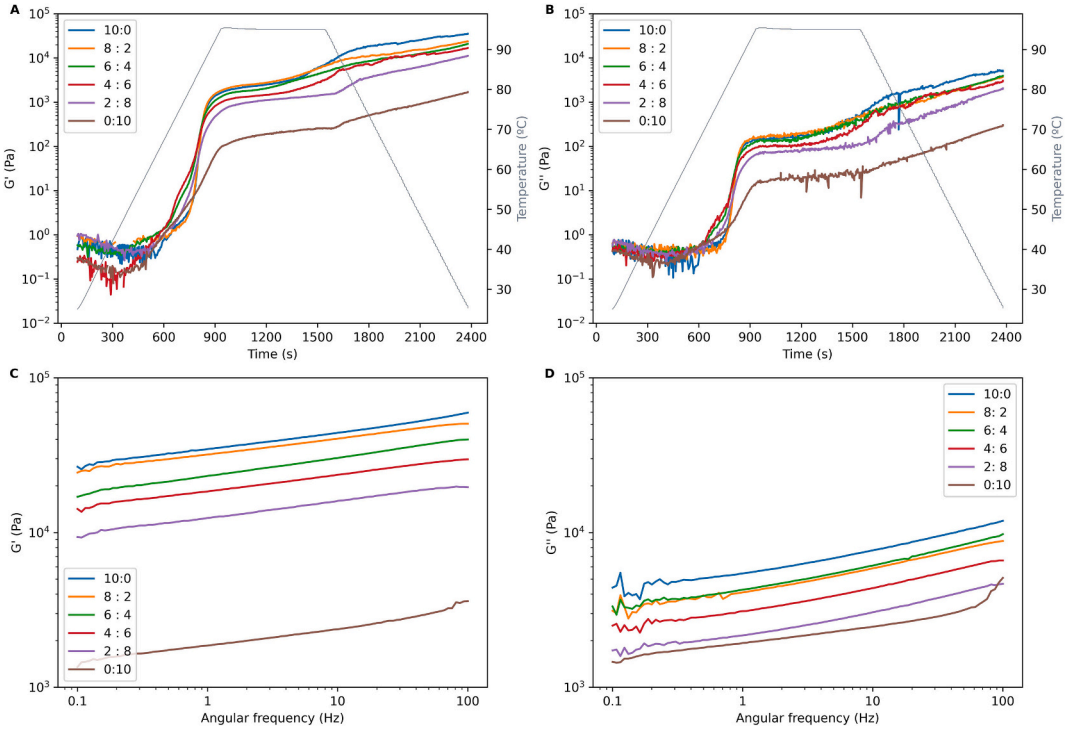

Fig. 2. Dynamic rheological behavior of the mixed EW-FP gelation in different protein ratios. Storage modulus (A), loss modulus (B) in the temperature sweep, storage modulus (C), and loss modulus (D) in the angular frequency sweep (The ratios in figures refer to the protein mass ratio of EW to FP).

Table 1
The onset temperatures of each region, final G' of temperature sweep, and Power-Law model fitting results (K′, n', R^2) based on the frequency sweep of the mixed EW-FP gels.

	10:0	8:2	6:4	4:6	2:8	0:10
Onset T°C (FP, °C)	N.D.	N.D.	46	46	N.D.	46
Onset T°C (ovotransferrin, °C)	66	64	63	62	62	N.D.
Onset T°C (ovalbumin, °C)	~79	~77	~73	~70	~73	N.D.
Final G' (Pa)	35,400	23,800	20,900	16,800	11,200	1710
K′ (Pa • s, × 10^3)	29.80 ± 1.69^{a}	24.24 ± 2.20^{b}	18.92 ± 0.34^{c}	14.74 ± 0.45^{d}	9.43 ± 0.78^{e}	1.46 ± 0.01^{f}
n'	0.10 ± 0.01^{b}	0.10 ± 0.00^{b}	0.11 ± 0.01^{ab}	0.11 ± 0.00^{b}	0.10 ± 0.00^{b}	0.13 ± 0.01^{a}
R^2	0.9965	0.9987	0.9992	0.9987	0.9975	0.9745

Note: The ratios refer to the protein mass ratio of EW to FP (Onset T°C: onset temperature. N.D.: not detected). Different letters in each row represent significant differences ($p < 0.05$).

3.2.2. *Surface hydrophobicity*

The proteins' surface hydrophobicity implies the tendency of protein molecules to adhere to one another in an aqueous environment (Alizadeh-Pasdar & Li-Chan, 2000), which is the driving force of gel formation. One percent EW-FP dispersions after heating were applied to simulate the intermediate stage of protein molecule/aggregates during the gelling process, so that the hydrophobic driving force for the gelation can be determined. It is assumed that the surface hydrophobicity can be predicted by the EW-FP ratios using the null model, where the total surface hydrophobicity is proportional to the number of hydrophobic groups and their affinity to ANS, and the value is the sum of the hydrophobicity of EW and FP, respectively (Cardamone & Puri, 1992; Kato & Nakai, 1980; Zhao et al., 2024). When the two proteins individually bind to ANS without affecting each other, the hydrophobicity values should be linear with the EW-FP ratio; otherwise, the extent of EW-FP interaction can be observed and quantified. Results of the surface hydrophobicity are shown in Fig. 3A, where the dashed lines signify the predicted linear change as a function of EW-FP ratios. Before heating, the EW group (3.49×10^6) exhibited significantly lower surface hydrophobicity than the FP group (13.91×10^6), and for the mixed groups, the changes highly aligned with the predicted values (except for 2:8, maybe due to the experimental variability), showing no EW-FP interactions when only mixing the two proteins. After heating, the surface hydrophobicity of all groups increased greatly, among which, the EW group was 55.37×10^6, which was higher than that of the FP group (39.10×10^6), indicating EW protein exposed more hydrophobic groups than FP under heating (Lee et al., 2024). Moreover, all EW-FP mixtures (8:2, 6:4, 4:6, and 2:8) exhibited higher values than the predicted linear trend, with the 6:4 and 4:6 ratios having the greatest deviations (5.59×10^6 and 5.98×10^6, respectively). These findings indicate that heating-induced EW-FP interactions resulted in extra increments of the surface hydrophobicity, approaching saturation between ratios of 6:4 and 4:6. Furthermore, the too-high hydrophobicity of protein can reduce the bonding with water, resulting in the low stability of the spatial structure of protein molecules, which can further accelerate the formation of hydrophobic aggregation and cause the 'too-fast' asynchronous gelation (Lee et al., 2024; Su et al., 2015; Xue et al., 2023). It also corresponded to the phenomenon in the rheological temperature sweep (section 3.2.1), where the pre-initiated denaturation and aggregation of ovotransferrin and ovalbumin, respectively, evidenced an accelerated gelation driven by the overexposure of hydrophobic groups. In addition, surface hydrophobicity showed significant correlations with gel hardness ($r = 0.83$, $p < 0.05$), final G' ($r = 0.90$, $p < 0.05$), and WHC ($r = -0.96$, $p < 0.01$), presenting a strong link between the process during the gel formation and the apparent properties. Therefore, it can be speculated that the excessively increased surface hydrophobicity was the direct outcome of the EW-FP interaction, which drove the change in gelling pattern and further affected the gelling properties.

3.2.3. *Intrinsic fluorescence*

One percent (*w*/w) of EW-FP dispersion was also exploited to determine the fluorescence of aromatic amino acids, represented by tryptophan (Trp), which has the strongest fluorescence at around 360 nm, that can signal protein conformational changes during the gelling process (Diana Kerezsi et al., 2024). As shown in Fig. 3B, before heating, the fluorescence intensity (FI) decreased with the increase of FP ratio due to EW having more aromatic amino acids than FP (Attia et al., 2020; David et al., 2024). After heating, two peaks were presented in groups 10:0 and 8:2, where the maximum fluorescence wavelengths were around 360 nm and 400 nm. Besides, all groups had increased FI after heating, and the increments of maximum fluorescence intensity decreased rapidly with the increase in FP content, where group 2:8 had the lowest increment of 3.60%, which is also lower than group 0:10 of 12.62%. Moreover, the first peaks of the groups 10:0 and 8:2 had blue

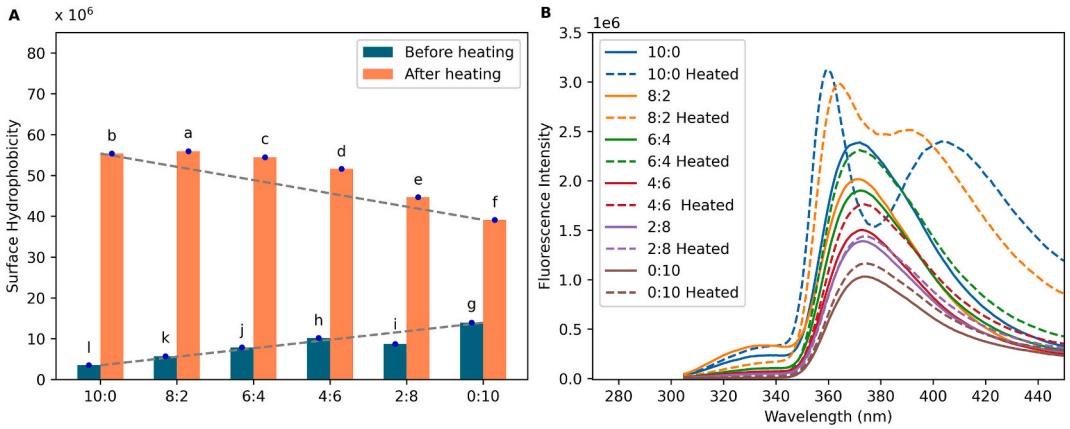

Fig. 3. The surface hydrophobicity (A) and intrinsic fluorescence (B) of 1% protein dispersions prepared from different ratios of EW-FP before and after heating (The ratios in figures refer to the protein mass ratio of EW to FP). The dashed line in (A) refers to the predicted linear change with the EW-FP ratio. Different letters in subplot (A) represent significant differences ($p < 0.05$).

shifts of around 12 nm and 8 nm after heating, respectively.

The second peak observed in groups 10:0 and 8:2 can be explained by the existence of the excimers during the EW gelation, where the excimer was formed by the combination of an aromatic residue in the excited state with another in the ground state, having a wide emission band between 400 and 480 nm (Bains et al., 2011; Keleti, 1970). This type of excimer potentially existed in all the EW-containing groups. In addition, the increased FI of all groups suggested that when proteins underwent unfolding, the Trp residues were exposed to a higher "non-polar" microenvironment with being surrounded by the adjacent hydrophobic groups or embedded in the formed EW-EW, FP-FP, or EW-FP aggregates instead of entering the aqueous phase and causing fluorescence quenching (Diana Kerezsi et al., 2024; Vivian & Callis, 2001). The increase of FI is also supported by the results of Zang et al. (2025), while on contrary to the study of Lee et al. (2024), where the 0.5 mg/mL EW solution were used and showed a decrease from 776.23 to 129.28 after 95 °C-heating, maybe due to the low protein concentration couldn't initiate the hydrophobic aggregation where the fluorescence was quenched by water.

Besides, the blue shifts of the first peak in groups 10:0 and 8:2 confirmed that the high "non-polar" microenvironment to which the Trp residues were exposed. When the FP content continued to increase, the "blue shift" of the EW protein part stopped accompanying the rapid decreases in FI increments (as proved by the lower increments in group 2:8 of 3.60% than 0:10 of 12.62%), indicating the asynchronous aggregation caused by EW-FP interaction hampered Trp residues linking to the hydrophobic groups, therefore, the gelation pattern was evidenced to be altered.

3.3. Structural characterization of gel matrix

3.3.1. Microstructure

As a consequence of the asynchronous protein aggregation promoted by the changes of protein's unfolding and the hydrophobic groups' exposure, the gel microstructure changed with the EW-FP ratio and was observed by SEM under magnification of 80 ×, 500 ×, and 3000 × as shown in Fig. 4. EW and FP gel had relatively fine and dense sectional profile under the magnification of 80 ×, 500 ×, and 3000 ×. EW had a structured network composed of small protein aggregates around 3–4 μm (Fig. 4A3), which were consistent with the images of Wang et al. (2020). In addition, FP gel showed an amorphous structure with smoother and larger aggregates stacked together (Fig. 4F3).

For the mixed groups, the images of groups 8:2, 6:4, and 4:6 in Fig. 2 (B1, C1, and D1) became much coarser, showing random larger protein clusters under 80 ×. With further increasing of FP, the group 2:8 (Fig. 2E1) presented the denser surface with less porosity which was closer to the FP gel. Moreover, pores can be observed under 500 × as marked by the circles (Fig. 4, B2, C2, D2, and E2), the group 8:2 had small and large pores in range from 10 μm to 50 μm diameter coexisting in the gel matrix, and group 6:4 had the largest pores over 130 μm, showing the most irregular structure. When the FP accounted for more, the pore sizes were increased, of 60–100 μm in group 4:6, and presented more dense structure with shallow pores around 50 μm in group 2:8. Under the magnification of 3000 × (Fig. 4, B3, C3, D3, E3), with the increase of the FP ratio, the backbone of the structure had been gradually substituted by the FP protein, and the surface of aggregates became smoother and thicker, the structure tended to diminish, while the FP came to dominate the gel structure as the gel appearance turned to neat from coarse, and less space was generated with the filling of FP.

Compared with the textural properties and G', the changes in gel strength were highly related to the density of the gel microstructure, where the generated irregular aggregates also weakened it. While the increase in springiness may be due to the heterogeneous structure providing more space for the protein strands when under deformation, the strands can spring back instead of being squeezed apart by mutual compression. Besides, under 500 × magnification, where the mixed groups showed porosity to different extents with the change of FP ratio, hence the greater proportion of the free water was stored in the pores rather than binding to the network, especially for group 6:4, which showed the most porosity and corresponded to the lowest WHC.

3.3.2. Middle-field infrared

The second derivative analysis was applied to quantify the relative percentage of the secondary structure of the mixed EW-FP gels based on the amide I region in the range of wavenumber 1700–1610 cm^{-1}. The α-helix, β-sheet, β-turn, random coil, and the unordered aggregate A1 and A2 were presented in Fig. 5. The α-helix content showed a synergistic growth in groups 8:2, 6:4, and then decreased with the increased FP ratio, respectively. The β-sheet and β-turn had a paired change where the β-sheet decreased significantly when it composed a high proportion of EW or FP in groups 8:2 and 2:8, where the content of β-turn showed a high percentage, presenting an opposite decrease-and-increase trend in the composite gels. The changes in the random coil were also similar to the trend in α-helix, exhibiting an inverted U-shaped trend. Besides, both unordered aggregates A1 and A2 had non-monotonic relationships with the EW-FP ratios. A1 accounted for less content in the composite gels, and A2 also exhibited fluctuating change, which acted similarly to the β-turn.

The unfolding of α-helix has a promotion to the formation of the network (Niu et al., 2025), and the heat treatment changes the hydrogen bonding to proceed the extension of α-helix, and its exposed terminal residues can be transited to the random coil and β-turn unfolded intermediate, which further facilitates the formation of β-hairpin connected by β-turn, the adjacent β-strands in β-hairpin can be interacted by each other to form the β-sheet (Carbonaro et al., 2008; Lee et al., 2024). As a consequence, the slightly increased α-helix content implied the unfolding was hindered by the EW-FP interaction in the mixed groups. Besides, the transition from β-turn to β-sheet was affected in groups 8:2 and 2:8. It can be inferred that the high proportion of EW or FP hampered the formation of β-sheet. According to the correlation analysis, Surface hydrophobicity had strong correlations with the proportions of α-helix ($r = 0.90$, $p < 0.05$), unordered A1 ($r = -0.88$, $p < 0.05$), and the random coil ($r = 0.98$, $p < 0.01$). This indicated that the interaction between EW and FP had a synchronous effect on the interconversion of secondary structures and the exposure of surface hydrophobic groups, evidencing the alteration of the gelation pattern. Besides, the significantly negative correlation between random coil and WHC ($r = -0.99$, $p < 0.01$) implied that the existence of unordered structure could reduce the uniformity of the gel network; thus, this may be a negative factor for textural properties and WHC.

3.3.3. Oscillatory frequency sweep

The frequency sweep results of the mixed EW-FP groups were presented in Fig. 2 (C and D). All groups showed frequency dependence, presenting higher viscoelasticity with the increase in frequency and "solid-like" behaviors, except for the FP gels, when the frequency reached around 100 Hz, G" exceeded G', showing more "liquid-like". The powder-law model ($G' = K' \times \omega^{n'}$) was curve-fitted to the frequency sweep results as shown in Table 1. K′ indicates the gel mechanical strength. EW and 8:2 showed similar K′ values, and for the further increase of the FP proportion, the gel strength decreased significantly, which significantly correlated to the hardness ($r = 0.970$, $P < 0.01$) and gumminess ($r = 0.93$, $P < 0.01$). n' represents the relative amount of covalent bonds (the closer the value is to zero, the more covalent bonds the sample has). According to the values of n', the EW gel had a significantly higher amount of covalent bonds than the FP gel. In most of the mixed groups, the slight increment of n' values implied that fewer covalent bonds than EW gel participated in the gel formation and maintained the gel structure. The covalent bonds in the gel matrix mainly refer to disulfide bonds (Wang et al., 2020), which cooperate with other non-covalent interactions to establish the gel network.

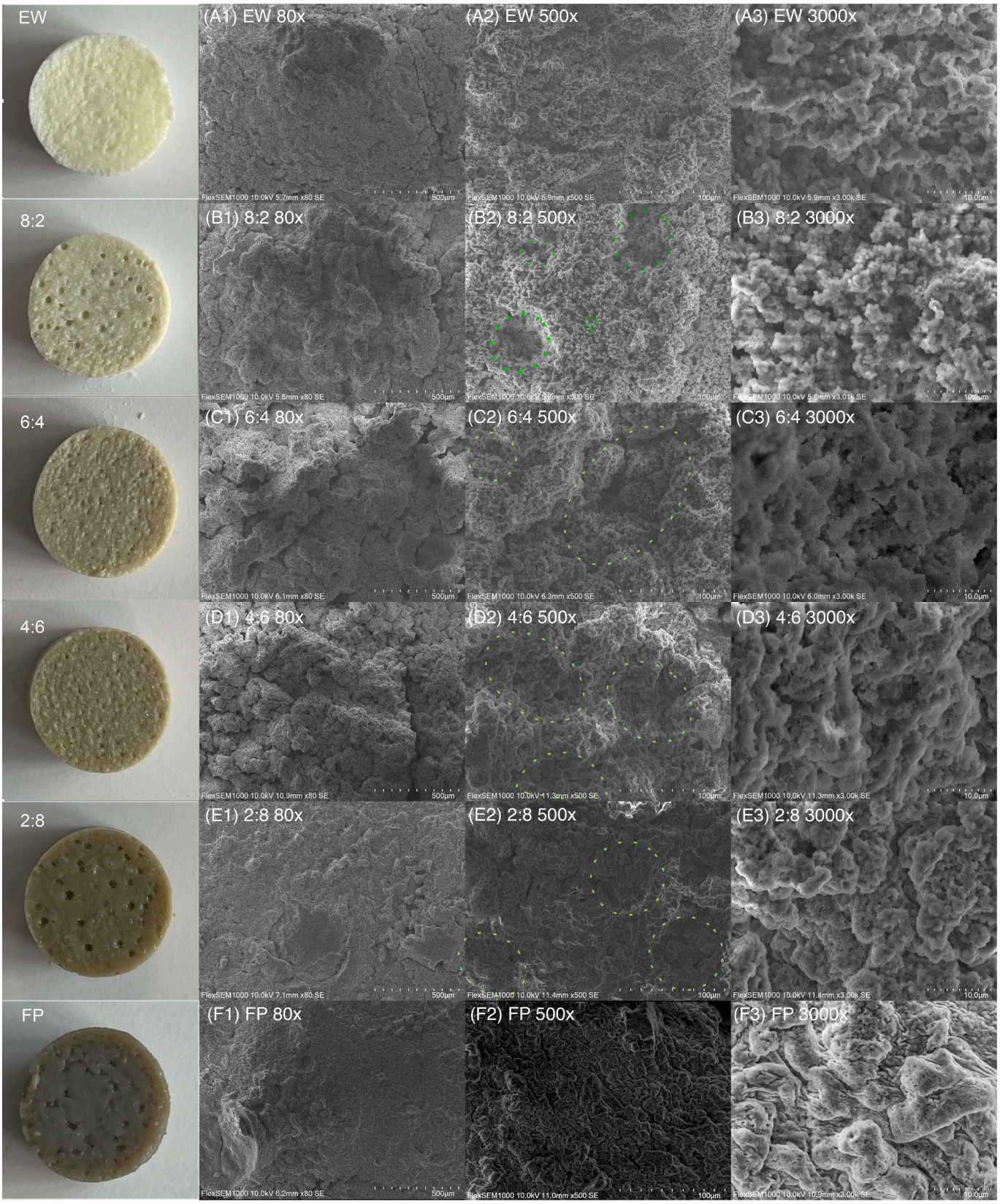

Fig. 4. The SEM images of mixed EW-FP gel observed under 80×, 500×, and 3000× magnification (The ratios in images refer to the protein mass ratio of EW to FP. Marco gel images are presented in the first column on the left side).

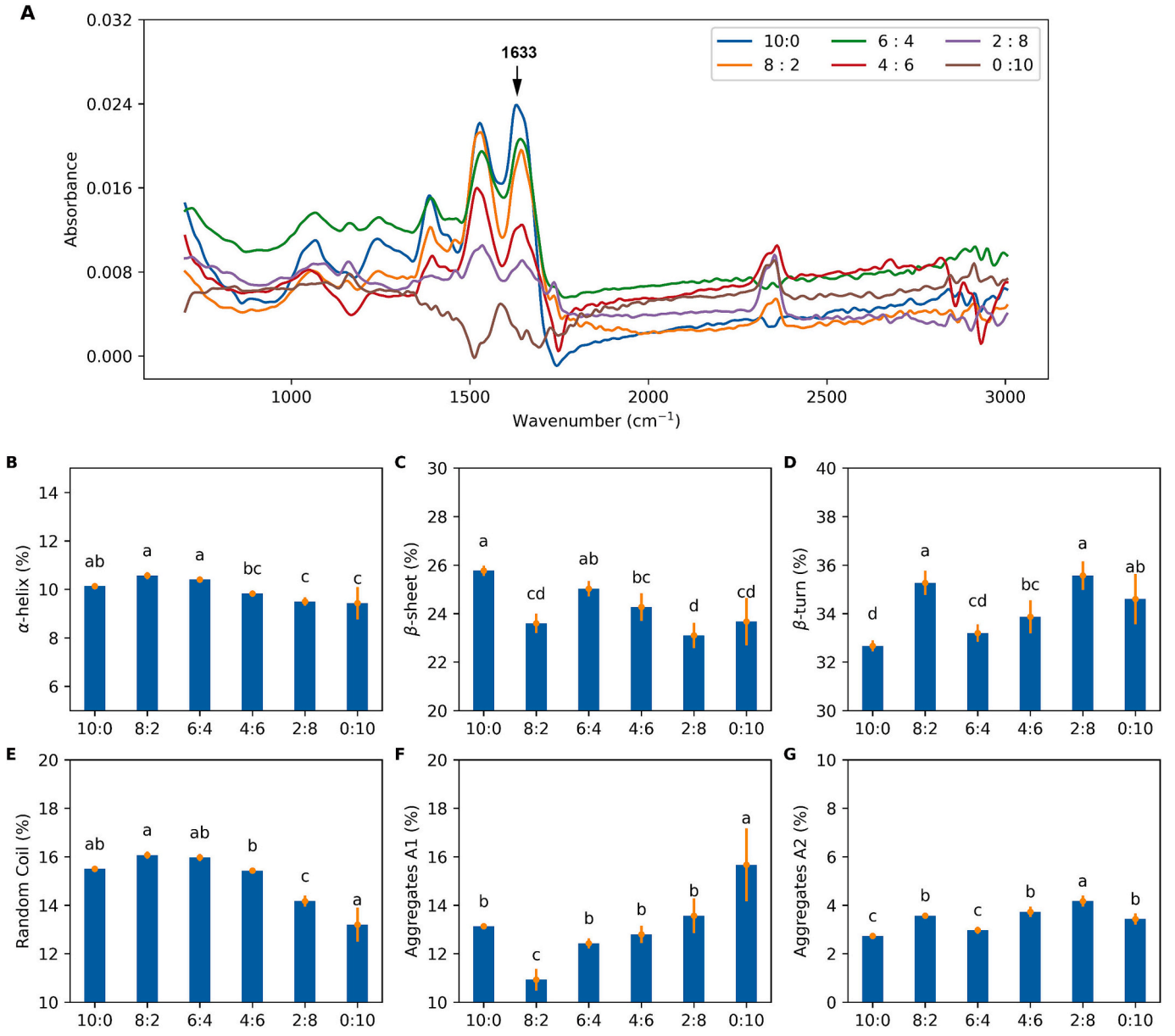

Fig. 5. Mid-infrared spectra of composite EW/FP gels (A). Percentage of the secondary structure of the composite EW-FP gels, alpha-helix (B), beta-sheet (C), beta-turn (D), random coil (E), aggregates A1 (F), and aggregates A2 (G) (The ratios in figures refer to the protein mass ratio of EW to FP). Different letters in each subplot (B–G) represent significant differences ($p < 0.05$).

Hence, the intermolecular forces were investigated to deeper demonstrate the gel structure and are detailed below.

3.3.4. *Intermolecular forces in gel*

The gel formation and the maintenance of its structure involved the linkages of covalent bonds, which mainly refer to disulfide bonds (Zhang et al., 2022), and non-covalent bonds, including electrostatic interaction, hydrogen bonds, and hydrophobic interaction etc. (Xia et al., 2022). These relative proportions of molecular interactions can be investigated by determining the gel solubility by screening each type of interaction. In Fig. 6A, the disulfide bonds, hydrophobic interaction & hydrogen bonds, and electrostatic forces in the EW gels were 73.61%, 22.82%, and 3.56%, respectively, where the disulfide bonds played a dominant role in maintaining the structure. Those of FP were 55.12%, 37.08%, and 7.80%, showing less difference between disulfide bonds and the "hydrophobic & hydrogen" than that of EW gels. The mixed gels, with the increase of FP content, had a decreasing trend in disulfide bonds proportion, and an increasing trend in "hydrophobic & hydrogen", which were 24.60%, 41.00%, 41.87%, and 57.04%, and it exceeded the disulfide bonds in the 2:8 group. Besides, the electrostatic interaction accounted for small proportions, also showing visible decreases in the mixed groups, where the 8:2 group had the lowest, 0.75%, and it continuously increased to 2.86% when the FP content was 80%.

In this experiment, the hydrophobic interaction and the hydrogen bonds were not separated to detect, due to the dissociative reagents such as SDS, urea, or guanidine hydrochloride, which can not only shield the hydrophobic interaction but also disrupt the hydrogen bonds, making it hard to detect each individually. Thus, the increment of the "hydrophobic & hydrogen" consisted of two changes. Xia et al. (2022) indicated that the higher surface hydrophobicity of the soy protein aggregates contributed to the enhancement of the hydrophobic interactions in gels. Similarly, the excessively increased surface hydrophobicity presented in section 3.2.2 potentially dominated the increase. Moreover, according to the results of WHC, the FP gels had excellent water binding capacity,

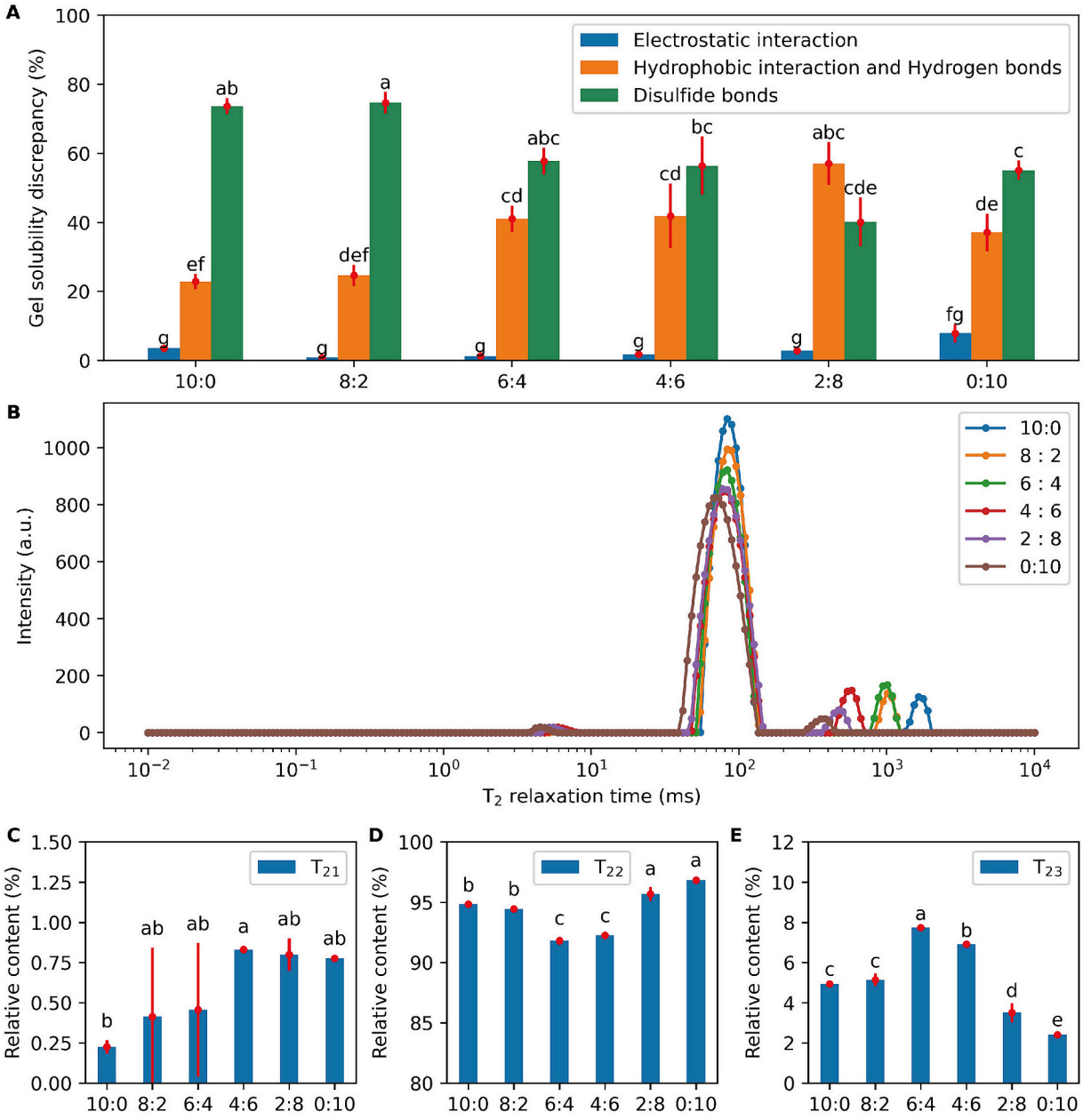

Fig. 6. Intermolecular forces in the composite EW-FP gels (A). T_2 relaxation time of composite EW/FP gels (B). The relative proportion of T_{21} (C), T_{22} (D), and T_{23} (E) (The ratios in figures refer to the protein mass ratio of EW to FP). Different letters in each subplot (A, C, D, and E) represent significant differences ($p < 0.05$).

implying that the hydrogen bonds could be increased with more FP content. Therefore, the changes of the "hydrophobic & hydrogen" in mixed gels were attributed to the increments of both.

For the heat-induced protein gelation without involving the ionic and enzymatic cross-linking, the disulfide bonds are considered the strongest attractive force positively correlating with the gel strength, followed by hydrophobic interactions, and the hydrogen bonds are regarded as weak forces, while electrostatic interaction is a repulsive force which acts between weak and strong depending on the ionic strength of the aqueous phase (Bryant & McClements, 1998; Hoffmann & van Mil, 1997).

The real amount of the disulfide bonds of the FP gel should be much lower than that of EW and gradually decrease in mixed groups with the increase in FP content due to the sulfur-containing amino acids, such as cysteine and methionine, account for 6.24% in EW (dry matter) (McNamara, 2013), while only 0.75–2.95% in FP (based on crude protein, dry matter) (David et al., 2024), which was roughly consistent with the n' value resulting in the low gel strength of FP presented in the gel hardness and G'. Combined with the proportions of the intermolecular force, the EW-FP interaction reduced the ratio of disulfide bonds and electrostatic interaction, meanwhile, enlarged the ratio of weaker forces (hydrophobic and hydrogen bonding) in mixed gels, causing heterogeneous microstructures, and further impaired the gel textural properties and rheological strength.

3.3.5. *Water distribution*

The water distribution can be determined by LF-NMR, where the T_2 relaxation time reflects the binding degree and the mobility of the water, which can be divided into bound water (T_{21}), generally stabilized by the hydrogen bonds; immobilized water (T_{22}), trapped within the network; and free water (T_{23}), presenting the peaks at 1–10 ms, 20–200 ms, and over 200 ms, respectively (Chen et al., 2025), as shown in Fig. 6B, The ratios of each peak area to the total indicating the proportions of the distribution, were exhibited in Fig. 6 (C, D, E). T_{21} accounted for a small

proportion (0.23–0.78%) of all groups, showing an increasing trend with the higher FP ratio. T_{22} was the main state of water distributing in EW-FP gels, since EW and FP groups had similar ratios of it (94.84% and 96.82%, respectively), and T_{23} was considered to have no interaction with protein, accounting for 4.94% and 2.40% in EW and FP gels, respectively. For the mixed groups, T_{22} showed lower proportions than those of both EW and FP gels and a "decrease-and-increase" with the increase in ratio of FP, reaching the low proportions at groups 6:4 and 4:6 of 91.80% and 92.25%, respectively. Correspondingly, the T_{23} exhibited a reversed trend, where groups 6:4 and 4:6 had the relatively higher proportions of 7.74% and 6.91%, respectively. Besides, the relaxation times of T_{21}, T_{22}, and T_{23} had shifts among all groups, which were shortened with the increase in FP ratio.

The increase in the ratio of FP accompanied by the increase of T_{21} indicated that more hydrogen bonds formed, which was consistent with the speculation in section 3.3.4, further proving that the FP was more capable of establishing hydrogen bonds with water. Besides, the shifts of the relaxation times also indicated that the FP had more binding degree with water and corresponded to the change of electrostatic interaction shown in Fig. 6A. The study of Zhang et al. (2015) also mentioned that the increase in negative electric charges would shorten the T_2 relaxation time to enhance the binding. Thereby, it can be speculated that the high WHC of FP was attributed to the high hydrogen bonding and high electrostatic interaction.

Furthermore, the decrease of the T_{22} in mixed groups exhibited that the water binding facilitated by hydrophilic residues was disrupted and reduced the limitation of water migration (Chen et al., 2025). Consequently, the free water accounted for more and existed in the pores of the gel matrix, evidenced by the changes of T_{23} proportions, which were highly consistent with the pore sizes observed in section 3.3.1, and also has strongly negative correlation with WHC ($r = -0.85$, $p < 0.05$). Thus far, the WHC losses can be concluded with two reasons: firstly, the asynchronous gelation caused by excessively increased surface hydrophobicity delivered a more porous structure, causing the higher proportion of free water; secondly, the deviations of the gel strength made the water more easily released by the mechanical deformation (Barbut, 1995).

4. Conclusion

The heat-induced EW-FP mixed gels at various ratios exhibited specific structural, textural, and rheological characteristics, including antagonistic reductions in hardness, resilience, cohesiveness, gumminess, but a synergistic enhancement of springiness. These effects were attributed to the EW-FP interactions, which modulated protein unfolding and aggregation during the thermal structuring. Specifically, the excessively exposed hydrophobicity accelerated the gelation process, which was characterized by the pre-initiated aggregation of the ovotransferrin and ovalbumin, respectively. This subsequently resulted in the formation of heterogeneous microstructures with high porosity. As well, the asynchronous gelation accompanied the changes in the intermolecular forces, where the proportion of strong covalent bonds (disulfide bonds) decreased, and the weaker hydrophobic interaction increased, which reduced the textural and rheological strength. Furthermore, the more porous microstructure, the higher proportion of free water, and the decreased gel strength collectively contributed to the loss of WHC in composite gels. The secondary structure was also affected due to the protein-protein interaction, where the changes in α-helix and random coil were synchronously increased with the change of surface hydrophobicity, which was detrimental to the uniformity of the gel network and presented strong correlations with gel strength and WHC.

Although antagonistic interactions were observed in the EW-FP gels, these findings provide a systematic understanding of partial substitution to mitigate formulation risks and also highlight the necessity of introducing appropriate process or structural modulation strategies, such as pH regulation, thermal control, and microfluidization, to regulate EW-FP interactions characterized by the over-increased surface hydrophobicity and further achieve optimal gelling properties. Furthermore, the distinctly porous structures observed in the 6:4 and 4:6 groups, combined with their higher springiness and greater free water content, could potentially be leveraged to impart a moist and palatable mouthfeel in gel products, including puddings, cakes, and sandwich cookies.

CRediT authorship contribution statement

Fangzhou Wang: Writing – review & editing, Writing – original draft, Visualization, Methodology, Investigation, Formal analysis, Data curation. **Romdhane Karoui:** Supervision, Methodology, Formal analysis. **Christophe Blecker:** Writing – review & editing, Validation, Supervision, Methodology, Investigation, Conceptualization.

Funding

This research did not receive any specific grant from funding agencies in the public, commercial, or not-for-profit sectors.

Declaration of competing interest

The authors declare that they have no known competing financial interests or personal relationships that could have appeared to influence the work reported in this paper.

Acknowledgments

The authors would like to thank Inès Othmeni (Univ. Artois, Arras, France), Imane Boukhers (Univ. Artois, Arras, France), and Jin Xie (Chinese Academy of Agricultural Sciences, Beijing, China) for their help with the protein structure characterization, Marjorie Servais (Teaching and research center, Gembloux, Belgium), Mariem Boukraâ (Teaching and research center, Gembloux, Belgium) and Audrey Haenen (Teaching and research center, Gembloux, Belgium) for the experimental material preparation, and Lynn Doran (Teaching and research center, Gembloux, Belgium), Arpita Chakraborty (Teaching and research center, Gembloux, Belgium), and Alfred Kouakou Kouassi (Teaching and research center, Gembloux, Belgium) for their professional technical support.

Appendix A. Supplementary data

Supplementary data to this article can be found online at https://doi.org/10.1016/j.foodchem.2026.148910.

Data availability

Data will be made available on request.

References

Alizadeh-Pasdar, N., & Li-Chan, E. C. Y. (2000). Comparison of protein surface hydrophobicity measured at various pH values using three different fluorescent probes. *Journal of Agricultural and Food Chemistry, 48*(2), 328–334. https://doi.org/10.1021/jf990393p

Alves, A. C., & Tavares, G. M. (2019). Mixing animal and plant proteins: Is this a way to improve protein techno-functionalities? *Food Hydrocolloids, 97*, Article 105171. https://doi.org/10.1016/j.foodhyd.2019.06.016

Attia, Y. A., Al-Harthi, M. A., Korish, M. A., & Shiboob, M. H. (2020). Protein and amino acid content in four Brands of Commercial Table Eggs in retail Markets in Relation to human requirements. *Animals : an Open Access Journal from MDPI, 10*(3), Article 406. https://doi.org/10.3390/ani10030406

Augustin, M. A., & Cole, M. B. (2022). Towards a sustainable food system by design using faba bean protein as an example. *Trends in Food Science & Technology, 125*, 1–11. https://doi.org/10.1016/j.tifs.2022.04.029

Bains, G., Patel, A. B., & Narayanaswami, V. (2011). Pyrene: A probe to study protein conformation and conformational changes. *Molecules, 16*(9), 7909–7935. https://doi.org/10.3390/molecules16097909

Barbut, S. (1995). Effect of sodium level on the microstructure and texture of whey protein isolate gels. *Food Research International, 28*(5), 437–443. https://doi.org/10.1016/0963-9969(95)00034-8

Blecker, C., Paquot, M., & Deroanne, C. (2000). Gelling properties of whey proteins after enzymic fat hydrolysis. *Journal of Food Science, 65*(4), 561–563. https://doi.org/10.1111/j.1365-2621.2000.tb16048.x

Bryant, C. M., & McClements, D. J. (1998). Molecular basis of protein functionality with special consideration of cold-set gels derived from heat-denatured whey. *Trends in Food Science & Technology, 9*(4), 143–151. https://doi.org/10.1016/S0924-2244(98)00031-4

Carbonaro, M., Maselli, P., Dore, P., & Nucara, A. (2008). Application of Fourier transform infrared spectroscopy to legume seed flour analysis. *Food Chemistry, 108*(1), 361–368. https://doi.org/10.1016/j.foodchem.2007.10.045

Cardamone, M., & Puri, N. K. (1992). Spectrofluorimetric assessment of the surface hydrophobicity of proteins. *Biochemical Journal, 282*(2), 589–593. https://doi.org/10.1042/bj2820589

Chen, Y., Cai, X.-L., Liu, L., Zhang, T., Qin, L.-K., & Jia, Y.-L. (2025). Preparation and performance characterization of insoluble dietary fiber-alginate-pea protein ternary composite gels. *Food Hydrocolloids, 160*, Article 110852. https://doi.org/10.1016/j.foodhyd.2024.110852

Croguennec, T., Renault, A., Beaufils, S., Dubois, J.-J., & Pezennec, S. (2007). Interfacial properties of heat-treated ovalbumin. *Journal of Colloid and Interface Science, 315*(2), 627–636. https://doi.org/10.1016/j.jcis.2007.07.041

David, L. S., Nalle, C. L., Abdollahi, M. R., & Ravindran, V. (2024). Feeding value of Lupins, field peas, Faba beans and chickpeas for poultry: An overview. *Animals : an Open Access Journal from MDPI, 14*(4), Article 619. https://doi.org/10.3390/ani14040619

Day, L. (2013). Proteins from land plants – Potential resources for human nutrition and food security. *Trends in Food Science & Technology, 32*(1), 25–42. https://doi.org/10.1016/j.tifs.2013.05.005

Diana Kerezsi, A., Jacquet, N., Lelia Pop, O., Othmeni, I., Figula, A., Francis, F., Karamoko, G., Karoui, R., & Blecker, C. (2024). Impact of pilot-scale microfluidization on soybean protein structure in powder and solution. *Food Research International, 188*. https://doi.org/10.1016/j.foodres.2024.114466

Dumoulin, L., Jacquet, N., Malumba, P., Richel, A., & Blecker, C. (2021). Dry and wet fractionation of plant proteins: How a hybrid process increases yield and impacts nutritional value of faba beans proteins. *Innovative Food Science & Emerging Technologies, 72*, Article 102747. https://doi.org/10.1016/j.ifset.2021.102747

Fernández-Quintela, A., Macarulla, M. T., Del Barrio, A. S., & Martínez, J. A. (1997). Composition and functional properties of protein isolates obtained from commercial legumes grown in northern Spain. *Plant Foods for Human Nutrition (Dordrecht, Netherlands), 51*(4), 331–342. https://doi.org/10.1023/a:1007936930354

Grasberger, K. F., Gregersen, S. B., Jensen, H. B., Sanggaard, K. W., & Corredig, M. (2021). Plant-dairy protein blends: Gelation behaviour in a filled particle matrix. *Food Structure, 29*, Article 100198. https://doi.org/10.1016/j.foostr.2021.100198

Guldiken, B., Stobbs, J., & Nickerson, M. (2021). Heat induced gelation of pulse protein networks. *Food Chemistry, 350*, Article 129158. https://doi.org/10.1016/j.foodchem.2021.129158

He, M., Zhang, M., Gao, T., Chen, L., Liu, Y., Huang, Y., Teng, F., & Li, Y. (2024). Assembly of soy protein-corn starch composite gels by thermal induction: Structure, and properties. *Food Chemistry, 434*, Article 137433. https://doi.org/10.1016/j.foodchem.2023.137433

Hoffmann, M. A. M., & van Mil, P. J. J. M. (1997). Heat-induced aggregation of β-Lactoglobulin: Role of the free thiol group and disulfide bonds. *Journal of Agricultural and Food Chemistry, 45*(8), 2942–2948. https://doi.org/10.1021/jf960789q

Hunter, J. D. (2007). Matplotlib: A 2D graphics environment. *Computing in Science & Engineering, 9*(3), 90–95. https://doi.org/10.1109/MCSE.2007.55

Johansson, M., Johansson, D., Ström, A., Rydén, J., Nilsson, K., Karlsson, J., Moriana, R., & Langton, M. (2022). Effect of starch and fibre on faba bean protein gel characteristics. *Food Hydrocolloids, 131*, Article 107741. https://doi.org/10.1016/j.foodhyd.2022.107741

Johansson, M., Karkehabadi, S., Johansson, D. P., & Langton, M. (2023). Gelation behaviour and gel properties of the 7S and 11S globulin protein fractions from faba bean (*Vicia faba* var. Minor) at different NaCl concentrations. *Food Hydrocolloids, 142*, Article 108789. https://doi.org/10.1016/j.foodhyd.2023.108789

Johansson, M., Karlsson, J., van den Berg, F. W. J., Ström, A., Ahrne, L., Sandström, C., & Langton, M. (2024). Effect of cellulose-rich fibres on faba bean protein gels is determined by the gel microstructure. *Food Hydrocolloids, 156*, Article 110295. https://doi.org/10.1016/j.foodhyd.2024.110295

Kato, A., & Nakai, S. (1980). Hydrophobicity determined by a fluorescence probe method and its correlation with surface properties of proteins. *Biochimica et Biophysica Acta (BBA) - protein. Structure, 624*(1), 13–20. https://doi.org/10.1016/0005-2795(80)90220-2

Keleti, T. (1970). The excimer fluorescence of tryptophan, tyrosine and d-glyceraldehyde-3-phosphate dehydrogenase. *FEBS Letters, 7*(3), 280–282. https://doi.org/10.1016/0014-5793(70)80181-8

Kim, G. H., & Chin, K. B. (2024). Effects of faba bean protein isolate on rheological properties of pork myofibrillar protein gels and quality characteristics of pork low-fat model sausages. *Journal of the Science of Food and Agriculture, 104*(10), 6322–6329. https://doi.org/10.1002/jsfa.13484

Kimura, A., Fukuda, T., Zhang, M., Motoyama, S., Maruyama, N., & Utsumi, S. (2008). Comparison of physicochemical properties of 7S and 11S globulins from pea, fava bean, cowpea, and French bean with those of soybean—French bean 7S globulin exhibits excellent properties. *Journal of Agricultural and Food Chemistry, 56*(21), 10273–10279. https://doi.org/10.1021/jf801721b

Kuang, J., Hamon, P., Lee, J., Bouhallab, S., Cases, E., Saurel, R., & Lechevalier, V. (2025). Protein–Protein interactions and structure of heat-set gels based on pea protein and egg white mixtures. *Gels, 11*(3), Article 176. https://doi.org/10.3390/gels11030176

Langton, M., Ehsanzamir, S., Karkehabadi, S., Feng, X., Johansson, M., & Johansson, D. P. (2020). Gelation of faba bean proteins—Effect of extraction method, pH and NaCl. *Food Hydrocolloids, 103*, Article 105622. https://doi.org/10.1016/j.foodhyd.2019.105622

Lee, S., Jo, K., Jeong, S.-K.-C., Jeon, H., Kim, Y.-J., Choi, Y.-S., & Jung, S. (2024). Heat-induced gelation of egg white proteins depending on heating temperature: Insights into protein structure and digestive behaviors in the elderly in vitro digestion model. *International Journal of Biological Macromolecules, 262*, Article 130053. https://doi.org/10.1016/j.ijbiomac.2024.130053

Li, J., Li, X., Wang, C., Zhang, M., Xu, Y., Zhou, B., Su, Y., & Yang, Y. (2018). Characteristics of gelling and water holding properties of hen egg white/yolk gel with NaCl addition. *Food Hydrocolloids, 77*, 887–893. https://doi.org/10.1016/j.foodhyd.2017.11.034

Li, J., Zhang, W., Tang, T., Gu, L., Su, Y., Yang, Y., Chang, C., & Han, Q. (2023). Thermal gelation and digestion properties of hen egg white: Study on the effect of neutral and alkaline salts addition. *Food Chemistry, 409*, Article 135263. https://doi.org/10.1016/j.foodchem.2022.135263

Li, L., Wang, Y.-Q., Zhang, L.-D., Yan, J.-N., Wang, C., Lai, B., & Wu, H.-T. (2025). Gelation properties and swallowing characteristics of heat-induced whey protein isolate/chia seed gum composite gels as dysphagia food. *Food Chemistry, 464*, Article 141712. https://doi.org/10.1016/j.foodchem.2024.141712

Lin, D., Lu, W., Kelly, A. L., Zhang, L., Zheng, B., & Miao, S. (2017). Interactions of vegetable proteins with other polymers: Structure-function relationships and applications in the food industry. *Trends in Food Science & Technology, 68*, 130–144. https://doi.org/10.1016/j.tifs.2017.08.006

Liu, X., Zhang, Z., Chen, Y., Zhong, M., Lei, Y., Huo, J., Ma, L., & Li, S. (2024). Chain reactions of temperature-induced egg white protein amorphous aggregates: Formation, structure and material composition of thermal gels. *Food Chemistry, 460*, Article 140785. https://doi.org/10.1016/j.foodchem.2024.140785

Ma, Y., Shan, A., & Chi, Y. (2023). Changes in structural, rheological, and gel properties of egg white protein induced by preheating in the dry state. *International Journal of Biological Macromolecules, 248*, 125851. https://doi.org/10.1016/j.ijbiomac.2023.125851

Manickavasagan, A., & Thirunathan, P. (2020). *Pulses: Processing and product development*. Springer International Publishing. https://doi.org/10.1007/978-3-030-41376-7

McNamara, D. J. (2013). Eggs. In B. Caballero (Ed.), *Encyclopedia of human nutrition* (3rd ed., pp. 132–138). Academic Press. https://doi.org/10.1016/B978-0-12-375083-9.00086-6.

Min, C., Ma, W., Kuang, J., Huang, J., & Xiong, Y. L. (2022). Textural properties, microstructure and digestibility of mungbean starch–flaxseed protein composite gels. *Food Hydrocolloids, 126*, Article 107482. https://doi.org/10.1016/j.foodhyd.2022.107482

Nahimana, P., Kerezsi, A. D., Karamoko, G., Abdelmoumen, H., Blecker, C., & Karoui, R. (2023). Impact of defatting methods on the physicochemical and functional properties of white lupin protein isolates. *European Food Research and Technology, 249*(9), 2387–2400. https://doi.org/10.1007/s00217-023-04305-x

Niu, F., Lin, C., Liao, H., Zhang, B., Zhang, J., & Pan, W. (2025). Formation mechanism of giant squid myofibrillar protein aggregates induced by egg white protein during heat treatment. *Food Hydrocolloids, 158*, Article 110573. https://doi.org/10.1016/j.foodhyd.2024.110573

Ozcan, I., Ozyigit, E., Erkoc, S., Tavman, S., & Kumcuoglu, S. (2023). Investigating the physical and quality characteristics and rheology of mayonnaise containing aquafaba as an egg substitute. *Journal of Food Engineering, 344*, Article 111388. https://doi.org/10.1016/j.jfoodeng.2022.111388

Punia Bangar, S., & Bala Dhull, S. (2022). *Faba bean: Chemistry, Properties and Functionality*. Springer International Publishing. https://doi.org/10.1007/978-3-031-14587-2

Rahate, K. A., Madhumita, M., & Prabhakar, P. K. (2021). Nutritional composition, anti-nutritional factors, pretreatments-cum-processing impact and food formulation potential of faba bean (*Vicia faba* L.): A comprehensive review. *LWT, 138*, Article 110796. https://doi.org/10.1016/j.lwt.2020.110796

Razi, S. M., Fahim, H., Amirabadi, S., & Rashidinejad, A. (2023). An overview of the functional properties of egg white proteins and their application in the food industry. *Food Hydrocolloids, 135*, Article 108183. https://doi.org/10.1016/j.foodhyd.2022.108183

Renzetti, S., van den Hoek, I. A. F., & van der Sman, R. G. M. (2020). Amino acids, polyols and soluble fibres as sugar replacers in bakery applications: Egg white proteins denaturation controlled by hydrogen bond density of solutions. *Food Hydrocolloids, 108*, Article 106034. https://doi.org/10.1016/j.foodhyd.2020.106034

Silva, J. V. C., Cochereau, R., Schmitt, C., Chassenieux, C., & Nicolai, T. (2019). Heat-induced gelation of mixtures of micellar caseins and plant proteins in aqueous solution. *Food Research International, 116*, 1135–1143. https://doi.org/10.1016/j.foodres.2018.09.058

Su, Y., Dong, Y., Niu, F., Wang, C., Liu, Y., & Yang, Y. (2015). Study on the gel properties and secondary structure of soybean protein isolate/egg white composite gels. *European Food Research and Technology, 240*(2), 367–378. https://doi.org/10.1007/s00217-014-2336-3

Team, T. Pandas Development. (2024). *Pandas-dev/pandas: Pandas (Version v2.2.2) [Computer software]. Zenodo*. https://doi.org/10.5281/zenodo.10957263

Thakur, G., Rodrigues, F. C., Dathathri, E., Nayak, S. K., & Pal, K. (2018). 2 - protein-based gels: Preparation, characterizations, applications in drug delivery, and tissue

engineering. In K. Pal, & I. Banerjee (Eds.), *Polymeric gels* (pp. 31–54). Woodhead Publishing. https://doi.org/10.1016/B978-0-08-102179-8.00002-8.

Urbonaite, V., van der Kaaij, S., de Jongh, H. H. J., Scholten, E., Ako, K., van der Linden, E., & Pouvreau, L. (2016). Relation between gel stiffness and water holding for coarse and fine-stranded protein gels. *Food Hydrocolloids, 56*, 334–343. https://doi.org/10.1016/j.foodhyd.2015.12.011

Virtanen, P., Gommers, R., Oliphant, T. E., Haberland, M., Reddy, T., Cournapeau, D., … van Mulbregt, P. (2020). SciPy 1.0: Fundamental algorithms for scientific computing in Python. *Nature Methods, 17*(3), 261–272. https://doi.org/10.1038/s41592-019-0686-2

Vivian, J. T., & Callis, P. R. (2001). Mechanisms of tryptophan fluorescence shifts in proteins. *Biophysical Journal, 80*(5), 2093–2109. https://doi.org/10.1016/S0006-3495(01)76183-8

Wang, C., Li, J., Li, X., Zhang, M., Gu, L., Chang, C., Su, Y., & Yang, Y. (2020). Molecular forces and gelling properties of heat-induced gel from egg white protein glycated with isomalto-oligosaccharide. *Food Hydrocolloids, 99*, Article 105356. https://doi.org/10.1016/j.foodhyd.2019.105356

Wu, C., Wang, T., Ren, C., Ma, W., Wu, D., Xu, X., Wang, L.-S., & Du, M. (2021). Advancement of food-derived mixed protein systems: Interactions, aggregations, and functional properties. *Comprehensive Reviews in Food Science and Food Safety, 20*(1), 627–651. https://doi.org/10.1111/1541-4337.12682

Wu, C., Yan, X., Wang, T., Ma, W., Xu, X., & Du, M. (2019). A self-sorted gel network formed by heating a mixture of soy and cod proteins. *Food & Function, 10*(8), 5140–5151. https://doi.org/10.1039/C9FO00560A

Xia, W., Zhu, L., Delahaije, R. J. B. M., Cheng, Z., Zhou, X., & Sagis, L. M. C. (2022). Acid-induced gels from soy and whey protein thermally-induced mixed aggregates: Rheology and microstructure. *Food Hydrocolloids, 125*, Article 107376. https://doi.org/10.1016/j.foodhyd.2021.107376

Xie, J., Bi, J., Jacquet, N., Blecker, C., Wang, F., & Lyu, J. (2024). Dysphagia food: Impact of soy protein isolate (SPI) addition on textural, physicochemical and microstructural properties of peach complex gels. *Food Hydrocolloids, 154*, Article 110130. https://doi.org/10.1016/j.foodhyd.2024.110130

Xue, H., Liu, H., Zhang, G., Tu, Y., & Zhao, Y. (2023). Formation mechanism of salted egg yolk mudding during storage: Protein oxidation, gel structure, and conformation. *Food Chemistry, 413*, Article 135632. https://doi.org/10.1016/j.foodchem.2023.135632

Ye, T., Chen, X., Li, Q., Chen, Z., Lin, L., Zheng, Z., & Lu, J. (2024). Towards more sustainable surimi gels: Deciphering the hybrid gelation of myofibrillar/plant proteins. *Food Hydrocolloids, 146*, Article 109189. https://doi.org/10.1016/j.foodhyd.2023.109189

Zang, J., Qing, M., Chi, Y., & Chi, Y. (2025). Egg white protein under thermal stress: Thermal aggregation orientation and gel properties decline. *International Journal of Biological Macromolecules, 295*, Article 139625. https://doi.org/10.1016/j.ijbiomac.2025.139625

Zhang, T., Yuan, Y., Chai, J., Wu, X., Saini, R. K., Liu, J., & Shang, X. (2022). How does dextran sulfate promote the egg white protein to form transparent hydrogel?The gelation mechanism and molecular force changes. *Food Hydrocolloids, 133*, Article 107901. https://doi.org/10.1016/j.foodhyd.2022.107901

Zhang, Z., Yang, Y., Tang, X., Chen, Y., & You, Y. (2015). Chemical forces and water holding capacity study of heat-induced myofibrillar protein gel as affected by high pressure. *Food Chemistry, 188*, 111–118. https://doi.org/10.1016/j.foodchem.2015.04.129

Zhao, Y.-R., Peng, N., Wang, C., Li, Y.-Q., Liang, Y., Guo, Z.-W., Sun, A.-Y., & Ren, X. (2024). Preparation and characterization of pea protein isolate-egg white protein composite gels. *Food Hydrocolloids, 148*, Article 109464. https://doi.org/10.1016/j.foodhyd.2023.109464

Zou, B., Zheng, X., Cai, W., Wan, W., Na, X., Du, M., & Wu, C. (2025). Pea proteins weaken pea-cod composite gel by forming a loose aggregate structure with diminished molecular interactions. *Food Hydrocolloids, 162*, Article 111009. https://doi.org/10.1016/j.foodhyd.2024.111009